



Connectomes from streamlines tractography: Assigning streamlines to brain parcellations is not trivial but highly consequential



Chun-Hung Yeh ^{a,*}, Robert E. Smith ^{a,b}, Thijs Dhollander ^{a,b}, Fernando Calamante ^{a,b,c}, Alan Connolly ^{a,b,c}

^a Florey Institute of Neuroscience and Mental Health, Melbourne, Victoria, Australia

^b Florey Department of Neuroscience and Mental Health, University of Melbourne, Melbourne, Victoria, Australia

^c Department of Medicine, Austin Health and Northern Health, University of Melbourne, Melbourne, Victoria, Australia

ARTICLE INFO

Keywords:

Diffusion MRI
Tractography
Structural connectome
Connectomics
Network metrics
Brain parcellation

ABSTRACT

When using diffusion MRI streamlines tractograms to construct structural connectomes, ideally, each streamline should connect exactly 2 regions-of-interest (i.e. network nodes) as defined by a given brain parcellation scheme. However, the ill-posed nature of termination criteria in many tractography algorithms can cause streamlines apparently being associated with zero, one, or more than two grey matter (GM) nodes; streamlines that terminate in white matter or cerebrospinal fluid may even end up being assigned to nodes if the definitions of these nodes are not strictly constrained to genuine GM areas, resulting in a misleading connectome in non-trivial ways. Based on both in-house MRI data and state-of-the-art data provided by the Human Connectome Project, this study investigates the actual influence of streamline-to-node assignment methods, and their interactions with fibre-tracking terminations and brain parcellations, on the construction of pairwise regional connectivity and subsequent connectomic measures. Our results show that the frequency of generating successful pairwise connectivity is heavily affected by the convoluted interactions between the applied strategies for connectome construction, and that minor changes in the mechanism can cause significant variations in the within- and between-module connectivity strengths as well as in the commonly-used graph theory metrics. Our data suggest that these fundamental processes should not be overlooked in structural connectomics research, and that improved data quality is not in itself sufficient to solve the underlying problems associated with assigning streamlines to brain nodes. We demonstrate that the application of advanced fibre-tracking techniques that are designed to correct for inaccuracies of track terminations with respect to anatomical information at the fibre-tracking stage is advantageous to the subsequent connectome construction process, in which pairs of parcellation nodes can be more robustly identified from streamline terminations via a suitable assignment mechanism.

1. Introduction

Diffusion MRI streamlines tractography is the main *in vivo* non-invasive technique for inferring mesoscale features of structural brain connectivity. This is typically achieved by constructing a connectome that uses streamlines connectivity linking the regions-of-interest (ROIs) defined by a brain parcellation scheme to provide a summary of putative white matter (WM) connections between pairs of grey matter (GM) regions (Bullmore and Sporns, 2009). The GM ROIs and the ‘strengths’ of such WM connections are often used as the basic elements, called nodes and edges respectively, to construct a graph that represents the topology of a brain network. The construction of a structural connectome typically

requires some mechanism to associate streamlines with GM ROIs. Given how fundamental this mechanism is to the construction process, the accuracy of such an underlying mechanism could have crucial impact on connectome construction as well as subsequent network properties.

In tractogram-based structural connectome construction, ideally each streamline should connect exactly two GM regions; however, in practice, conventional fibre-tracking algorithms and streamline-to-node assignment mechanisms often result in streamlines being associated with zero, one, or more than two GM regions. Previous studies have reported that the amount of such ‘unassignable’ streamlines (i.e. connecting zero or only one node) can reach ~33–50% (Hagmann et al., 2008) or even up to ~80% (Zalesky et al., 2010) of the total streamlines generated at the

* Corresponding author. The Florey Institute of Neuroscience and Mental Health, Melbourne Brain Centre, 245 Burgundy Street, Melbourne, VIC, 3084, Australia.
E-mail addresses: chun-hung.yeh@florey.edu.au, jimmy.chyeh@gmail.com (C.-H. Yeh).

fibre-tracking stage. Even though these unassignable streamlines do not have any contribution to the subsequent structural network, treating the remaining streamlines that are ‘assignable’ to at least two network nodes as a complete representation of WM connectivity may incur various biases. Furthermore, since some parcellation schemes do not constrain brain nodes strictly to GM voxels – such as the widely-used AAL atlas, in which the nodes incorporate significant portions of brain WM (Tzourio-Mazoyer et al., 2002) – streamlines that terminate within WM may be included in connectome construction, despite that such premature termination fails to properly reconstruct GM-GM connectivity. Given a basic understanding of how neurons are arranged within the brain, it is reasonable to suggest that since neuronal axons do not terminate in the middle of a WM region, then a streamline that does this cannot be representative of any biological connection. Such apparent ‘connectivity’ is not biologically meaningful, and could therefore result in a misleading connectome in non-trivial ways. However, despite the growing popularity of structural connectomics research, the practical consequences of the fundamental mechanism for assigning streamlines to relevant brain network nodes have not yet been determined.

To investigate the effects of the method used to identify pairwise connections between brain nodes, this study focuses on three confounding factors that could have significant influence on structural connectome construction; namely:

- **Brain parcellation scheme** – The efficacy of identifying pairwise streamline connectivity is not independent of the brain parcellation scheme being used, but is expected to be influenced in particular by the spatial extent enclosed by a brain parcel. For example, in two of the most commonly-used image-based parcellation schemes, the Desikan-Killiany atlas (Desikan et al., 2006) and the AAL atlas (Tzourio-Mazoyer et al., 2002), the former constrains voxel-wise labelling of nodes to GM voxels only, whereas in the latter those labels extend into WM voxels.
- **Track termination criteria** – Premature termination of the fibre-tracking process within WM or cerebrospinal fluid (CSF), or propagation of streamlines through and beyond the cortical GM, often occurs in tractography algorithms that terminate streamlines only on the basis of empirical constraints such as local streamline curvature, diffusion anisotropy (e.g. fractional anisotropy), or fibre orientation distribution (FOD) amplitude, without consideration of the underlying brain tissue anatomy. Since these tractography methods do not systematically generate inter-areal connections between GM, many resultant streamlines are unlikely to be appropriately assigned to a pair of brain nodes.
- **Node assignment mechanism** – This refers to the method used to assign a given streamline to the associated brain nodes. Most studies simply use the label ascribed to the voxel in which the streamline termination resides (e.g. (Hagmann et al., 2008; Zalesky et al., 2010)), while some studies consider every node intersected by a streamline trajectory (e.g. (Lo et al., 2010)). Intuitively, the selection of what mechanism to use for this purpose might have a direct impact on connectome quantification; however, the practical influence of the node assignment process has not been evaluated before.

The issues related to the construction of pairwise structural connections can be in principle improved by using advanced tractography techniques such as anatomically-constrained tractography (ACT) (Smith et al., 2012) or similar variants (Girard et al., 2014). These methods improve the robustness and biological plausibility of streamline terminations by incorporating prior anatomical information provided by high-resolution anatomical images into the fibre-tracking process. They effectively prevent biologically unrealistic connections, such as those terminating inside WM or entering CSF, by constraining the termination of every streamline to occur only near the interface between grey and white matter (abbreviated to GM-WM interface, or GMWMI), within the subcortical GM, or at the spinal column (Girard et al., 2014; Smith et al.,

2012). Following the application of ACT, it has been demonstrated that ~90% of streamlines can be assigned to a pair of brain nodes from track endpoints, when assigning streamlines to nodes based on a 2 mm-radius search in the proximity of each streamline termination (Smith et al., 2015a). Although it is reasonable to assume that such construction should be more biologically accurate, the practical comparisons to other mechanisms using different parcellation schemes or node assignment approaches have not yet been evaluated.

In this work, we investigate the influence of node assignment mechanisms and their interactions with two popular parcellation schemes for identifying pairwise connectivity between nodes. In order to assess whether such mechanisms have significant implications for connectome quantification, we perform statistical comparisons among the strengths of modular connectivity and the graph theory metrics derived from different connectome construction strategies. In addition, improving MRI data quality is presumed to be advantageous to the construction of pairwise connections as well as to the accuracy of an individual's brain parcellation, thereby being beneficial to connectome construction. Given the growing applications of the MRI datasets released by the Human Connectome Project (HCP) (Glasser et al., 2013; Van Essen et al., 2013), this study also investigates whether the issues surrounding construction of pairwise structural connectivity can be overcome by using high quality MRI datasets, or if more rigorous strategies are fundamentally required for streamline-to-node assignment and structural connectomics.

2. Methods

2.1. MRI acquisition

2.1.1. In-house data

Twenty-two healthy volunteers were recruited in this study (number of females/males = 11/11; 32.5 ± 6.5 years old; all right-handed) with written informed consent obtained from all participants. All protocols were approved by the local Institutional Review Board. MRI data were acquired using a Siemens 3T Tim Trio system (Erlangen, Germany). T1-weighted images (T1WIs) were acquired using the 3D magnetization-prepared rapid gradient echo (MPRAGE) sequence (Mugler and Brookeman, 1990) with TR/TE/TI = 1900/2.6/900 ms, flip angle = 9°, field-of-view (FOV) = 230×230 mm², matrix size = 256×256 , 192 sagittal slices, 0.9 mm isotropic resolution. Diffusion-weighted images (DWIs) were acquired using a twice-refocused spin-echo echo-planar imaging sequence (Reese et al., 2003) with the following parameters: TR/TE = 8400/110 ms, parallel acceleration factor = 2, phase partial Fourier = 6/8, FOV = 240×240 mm², matrix size = 96×96 , 60 axial slices at 2.5 mm isotropic voxel dimension, $b = 3000$ s/mm² along 60 diffusion gradient directions, and 8 $b = 0$ images. An additional pair of $b = 0$ images with opposing phase encoding polarity was acquired for the estimation and correction of susceptibility induced image distortions (Andersson et al., 2003).

2.1.2. HCP data

The preprocessed structural and diffusion MRI datasets of ten subjects were downloaded from the ConnectomeDB (<https://db.humanconnectome.org>). The subjects were scanned using a Siemens 3T Connectome Skyra system. T1WIs were acquired using the 3D MPRAGE sequence at 0.7 mm isotropic resolution with TR/TE/TI = 2400/2.14/1000 ms, flip angle = 9°. Multi-shell DWIs were acquired using a 2D spin-echo single-shot multiband EPI sequence at 1.25 mm isotropic resolution, with TR/TE = 5500/89 ms, $b = 1000, 2000$, and 3000 s/mm² along 90 gradient directions for each b -value, and 18 $b = 0$ images. See (Glasser et al., 2013; Van Essen et al., 2013) for HCP data acquisition details.

2.2. Data processing

The following subsections describe the procedures for MRI data analysis. Data were principally processed using MRtrix3 (<https://www.mrtrix3.org>)

rtrix.org; version: release candidate 3) (Tournier et al., 2019); other relevant software tools are referred to specifically where used.

2.2.1. Preprocessing

For the in-house data, DWIs were processed to correct for susceptibility distortions, eddy currents, and inter-volume motion using FSL's (version: 5.0.9) TOPUP and EDDY tools (Andersson et al., 2003; Andersson and Sotropoulos, 2016; Smith et al., 2004). The B_1 bias field was corrected based on the mean $b=0$ image using the N4 algorithm (Tustison et al., 2010). After DWI corrections, the subjects' T1WIs were registered to the mean $b=0$ image via rigid-body transformations using SPM12 (<http://www.fil.ion.ucl.ac.uk/spm>). For the HCP data, the relevant steps for image distortion corrections and alignment had been done through the HCP pre-processing pipelines (Glasser et al., 2013). The N4 bias field correction method was applied additionally to correct for the intensity inhomogeneity (Tustison et al., 2010).

2.2.2. Brain parcellation scheme

Two popular atlas-based parcellation schemes were evaluated in individuals' T1WI spaces through the following procedure: (1) **FreeSurfer parcellation** – For the in-house data, the default FreeSurfer (version: 6.0.0) reconstruction pipeline (Dale et al., 1999) was performed on subjects' T1WIs with 84 parcels defined using the Desikan-Killiany cortical atlas segmentation (Desikan et al., 2006); the same parcellation scheme is also provided in the preprocessed HCP data. For all subjects, the subcortical structures labelled by FreeSurfer were refined by the subcortical GM segmentation obtained using FSL's FIRST tool (Patenaude et al., 2011; Smith et al., 2015a). (2) **AAL atlas** – The AAL atlas (Tzourio-Mazoyer et al., 2002), consisting of 116 areas, was transformed to individuals' T1WI space using SPM12's spatial normalisation and deformation tools (Friston et al., 2007). **For both parcellation schemes, an additional ROI was manually defined per subject in order to encompass streamlines transitioning from brainstem into spinal cord.**

2.2.3. Tractogram reconstruction

For both datasets, partial volume maps (PVMs) of brain tissues were estimated from the T1WIs in order to serve as anatomical information in ACT (Smith et al., 2012); this process includes segmentation of WM, GM, and CSF using FSL's FAST algorithm (Zhang et al., 2001), and subcortical GM structures estimated using FSL's FIRST tool (Patenaude et al., 2011) mapped from surface to image representation using a PVM estimation algorithm (Smith et al., 2012).

For the in-house data, FODs were estimated using constrained spherical deconvolution (CSD) (Tournier et al., 2007, 2008) with default parameters and a maximum spherical harmonic order of 8. Probabilistic fibre tractography was performed using the 2nd order integration over fibre orientation distributions (iFOD2) algorithm (Tournier et al., 2010) with a step size equal to half the voxel size, maximum curvature = 45° per step, length = 5–250 mm, and FOD amplitude threshold = 0.1. For each scan, tractograms of 10^7 streamlines were generated through the dynamic seeding technique (Smith et al., 2015b), and tracking either with or without ACT. The “back-tracking” mechanism was used within the ACT framework (Smith et al., 2012).

For the HCP data, FODs were computed using multi-shell multi-tissue (MSMT) CSD in which tissue response functions for GM, WM, and CSF were estimated from the multi-shell DWIs based on T1WI segmentation (Jeurissen et al., 2014). The same tractogram reconstruction approach was repeated for ACT and non-ACT, except that the FOD threshold for terminating tracking was reduced to 0.06 due to the ability of MSMT-CSD to reduce spurious FOD lobes (Jeurissen et al., 2014).

2.2.4. Connectome construction

In this study, we investigate three mechanisms (illustrated in Fig. 1) used to assign a given streamline to the relevant network nodes; they are denoted hereafter as:

- (1) **“All voxels”** = Test all voxels intersected along the path of a streamline (Lo et al., 2010);
- (2) **“End voxels”** = Test only the two voxels in which the streamline endpoints reside (Hagmann et al., 2008; Zalesky et al., 2010);
- (3) **“Local search”** = From each streamline endpoint, perform a search to locate the nearest labelled voxel, provided that voxel is within a 2 mm distance to the streamline endpoint (Smith et al., 2015a).

Note that for the “all voxels” mechanism, any given streamline intersecting a total number of n unique nodes ($n \geq 2$) contributes to $\frac{n!}{2(n-2)!}$ different edges in the connectome (one for each unique pair of nodes within the set of intersected nodes for that streamline); conversely, for both “end voxels” and “local search” approaches, the maximum number of nodes associated with a streamline is 2 (since the node assignment process considers only the 2 endpoints of each streamline), resulting in that streamline contributing to either zero or at most a single edge.¹

In summary, $2 \times 2 \times 3 = 12$ structural connectomes were generated for each subject using all combinations of: 2 tractography methods (non-ACT or ACT), 2 brain parcellation schemes (FreeSurfer or AAL), and 3 node assignment mechanisms (“all voxels”, “end voxels”, or “local search”). In order to make the quantification of streamline connectivity biologically meaningful, SIFT2 was applied to modulate the contribution weight of each streamline respecting the underlying FOD amplitudes (Smith et al., 2015b), i.e. the apparent fibre density (Raffelt et al., 2012). In this study, the connectome edge weight was defined as the sum of the relevant streamline weights provided by the SIFT2 model, i.e. a ‘weighted’ streamline count.

2.3. Connectivity analysis

2.3.1. Histogram of streamline connections

For every streamline of the tractogram data, the associated network nodes were recorded based on a given node assignment mechanism and a brain parcellation scheme; the group-averaged frequency of node count per streamline was then plotted as a histogram. This procedure was repeated for 12 connectome construction mechanisms mentioned above for both in-house and HCP datasets.

2.3.2. Default mode network connectivity

The comparisons of the connectomes generated from different construction strategies were conducted via assessing the connection strengths of a brain functional module, the default mode network (DMN). To this end, all the connectomes were post-processed to exclude both the cerebellum and intra-node connectivity, and thus the final connectomes were 82×82 and 90×90 matrices for FreeSurfer parcellations and the AAL atlas respectively (with diagonal entries all zero). The most common structures involved in DMN including precuneus, anterior cingulate, posterior cingulate, inferior parietal cortex, and medial prefrontal cortex were considered (Buckner et al., 2008) (see also Supplementary Table 1 for the relevant structural labels of DMN for both parcellation schemes). For each connectome, the strength within DMN ($S_{\text{DMN-intra}}$) and the strength between DMN and the rest of brain regions ($S_{\text{DMN-inter}}$) were computed by the sum of relevant edge values.

2.3.3. Graph theory metrics

The Brain Connectivity Toolbox (version: 2017-15-01) (Rubinov and Sporns, 2010) was used to compute network density (ρ) and weighted network metrics including strength (K^W), betweenness centrality (B^W),

¹ Note that when using “end voxels” or “local search”, we consider that a streamline successfully connects 2 nodes even if both endpoints are associated with the same node; however, when using “all voxels” assignment, a 2-node connection means that a streamline has intersected 2 *unique* nodes, i.e. even if both endpoints of a streamline reside within the same node, that streamline is considered to be associated with 1 node only.

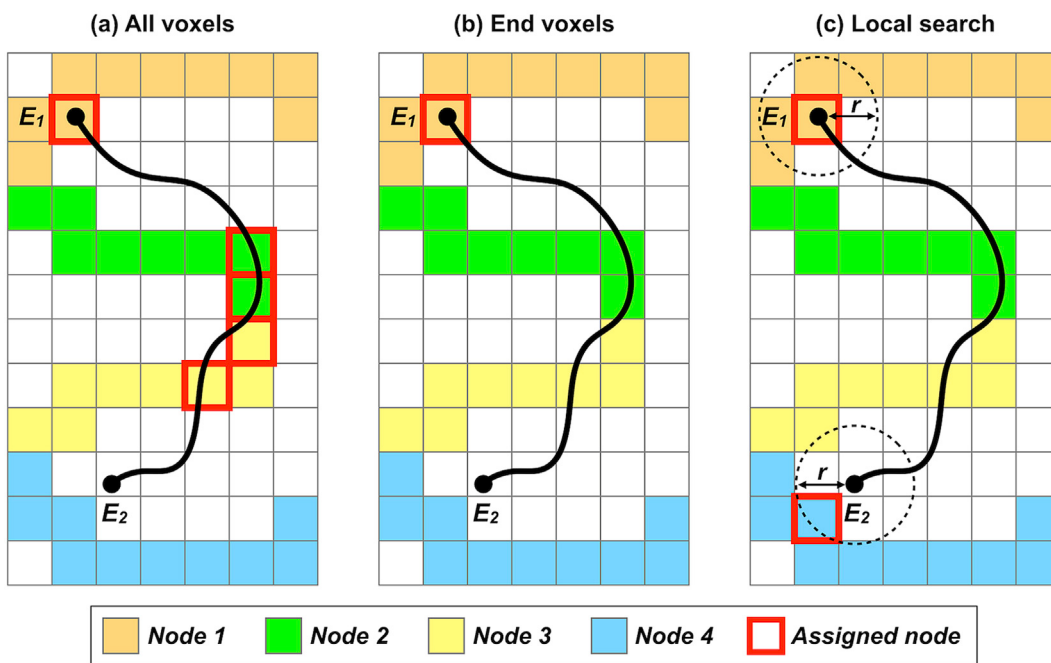


Fig. 1. Illustration of three node assignment mechanisms used to assign streamlines to network nodes. Streamlines shown in black; streamline endpoints denoted as E_1 and E_2 ; network nodes shown as coloured voxels. (a) “All voxels” looks for any visited node voxel along the streamline trajectory. In this example, the streamline visits three independent nodes (i.e. Node 1, 2, and 3), contributing to three pairs of network edges between Nodes 1 & 2, Nodes 1 & 3, and Nodes 2 & 3. (b) “End voxels” assigns the nodes purely based on the voxels where the endpoints of a streamline reside. In this case, the streamline is assigned to only one node (i.e. Node 1) at E_1 , and hence would not contribute to connectivity within the connectome. (c) “Local search” identifies the nearest nodes within a radius r from streamline endpoints. The example streamline is assigned to Node 1 and 4 at endpoints E_1 and E_2 respectively. Note that this simple demonstration reveals that the selection of node assignment mechanism has direct influence on connectome quantification.

characteristic path length (L^W), global efficiency (E_G^W), and local efficiency (E_L^W). Clustering coefficient (C^W) was additionally calculated based on the method described in (Zhang and Horvath, 2005). The superscript ‘ W ’ of these metric abbreviations indicates ‘weighted’ as opposed to those computed from a binary (i.e. ‘unweighted’) connectome. For each node-wise network measure (i.e. K^W , B^W , C^W , and E_L^W), the average of the metric over all nodes was calculated to obtain a global network property.

2.3.4. Statistical analysis

Statistical analyses of structural connectivity were performed using MATLAB (The MathWorks Inc., Natick, MA). A series of two-tailed t-tests were performed on the connectivity strengths of DMN and the graph theory metrics, to assess whether these network measures were significantly affected by the streamline termination criteria (i.e. non-ACT versus ACT; repeated for each assignment mechanism) and the node assignment methods (i.e. “all voxels” versus “end voxels”, “all voxels” versus “local search”, and “end voxels” versus “local search”; repeated for non-ACT and ACT). Hence for each metric, a total number of nine paired t-tests were conducted; we used the Bonferroni correction to account for multiple comparisons, with statistical significance at p -value = 0.05/9. Note that the correction was not performed among the network metrics since such a correction may not be valid for measures with various levels of correlations. Statistical comparisons between the parcellation schemes were not performed since no direct correspondence exists between the FreeSurfer parcellations and the AAL atlas.

3. Results

3.1. Histogram of streamline connections

Fig. 2 shows the group-averaged histograms of node count per streamline for the in-house data based on the 12 connectome

construction strategies as described in Methods. The results of each specific mechanism are summarised as follows:

- **Brain parcellation scheme** – For all cases, using the AAL atlas resulted in more 2-node connections than using FreeSurfer’s parcellation. The parcellation scheme had a dominant effect on the frequency of generating 2-node connections particularly for the “all voxels” and “end voxels” mechanisms: when using the AAL atlas with “all voxels” (Fig. 2(a)), the proportion of streamlines connecting ≥ 2 nodes reached $\sim 45\%$ without ACT and $\sim 75\%$ with ACT, which was higher than $\sim 20\%$ without ACT and $\sim 15\%$ with ACT when using FreeSurfer parcellations; when using “end voxels” (Fig. 2(b)) either with or without ACT, $< 35\%$ of streamlines were assigned to 2 nodes for the FreeSurfer parcellation, whereas $\sim 70\%$ of streamlines connect to 2 nodes for the AAL atlas. Likewise, the dependency on the parcellation scheme also exists for the “local search” mechanism, where 2-node connections were observed to be $\sim 70\%$ (FreeSurfer parcellation) and $\sim 80\%$ (AAL parcellation) when ACT was not used. However, such dependency on parcellation scheme was minimised when ACT was used in conjunction with the “local search” mechanism, by which the amount of 2-node connections reached up to $\sim 90\%$ for both FreeSurfer and AAL parcellations.
- **Tracking termination criteria** – The frequency with which streamlines were assigned to 2 nodes was higher with ACT than without ACT for all conditions, with the exception of combining FreeSurfer’s parcellation with “all voxels” (Fig. 2(a)) or “end voxels” (Fig. 2(b)). The highest frequency of 2-node connections occurred when ACT was combined with “local search” (Fig. 2(c)), regardless of the parcellation scheme used.
- **Node assignment mechanism** – When using “all voxels” or “end voxels”, the majority of streamlines were connected to 0 or only 1 node for FreeSurfer’s parcellation, whether or not ACT was used. The amount of 2-node connections was higher for the AAL atlas than the FreeSurfer parcellation, particularly when using “end voxels”, suggesting

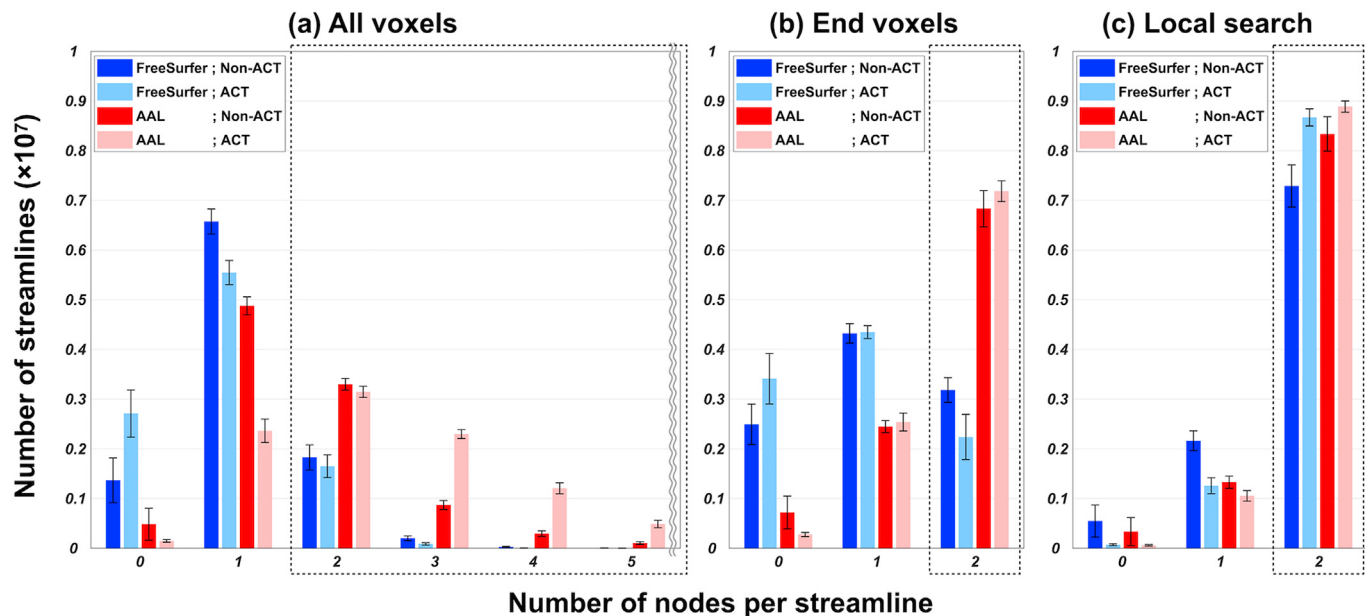


Fig. 2. Histograms of node count per streamline derived from the in-house data following 12 connectome construction strategies, where streamlines were assigned to brain nodes based on the (a) “all voxels”; (b) “end voxels”; (c) “local search” assignment mechanisms (see Methods 2.2.D for detailed descriptions). The horizontal axis shows the node count, and the vertical axis shows the group-averaged streamline count (mean \pm standard deviation). The dotted box shown in each plot indicates that the relevant streamlines have actual contributions to the outcome connectivity matrices.

that the results obtained using these two assignment approaches is strongly dependent on the parcellation scheme. When using “local search”, $\sim 70\%-80\%$ of streamlines connected two nodes for both parcellation schemes even without ACT, which was higher than when using “end voxels”. As reported above, the frequency of 2-node connections reached the maximum observed $\sim 90\%$ when the tractograms were generated using ACT and the “local search” mechanism was used.

Fig. 3 shows the group-averaged histograms obtained from the high-quality HCP data. While some mild increases in the frequency of 2-node

connections are observed, the overall trends are similar to the histograms derived from the lower quality in-house data across all connectome construction strategies. Again, in the case where FreeSurfer parcellation nodes were assigned using the “end voxels” mechanism, 2-node connections were more frequent without ACT than with (see Figs. 2(b) and 3(b)).

3.2. Connectomes

Fig. 4 illustrates the group-averaged connectivity matrices for the 12 types of connectome construction for both MRI datasets. As expected, the

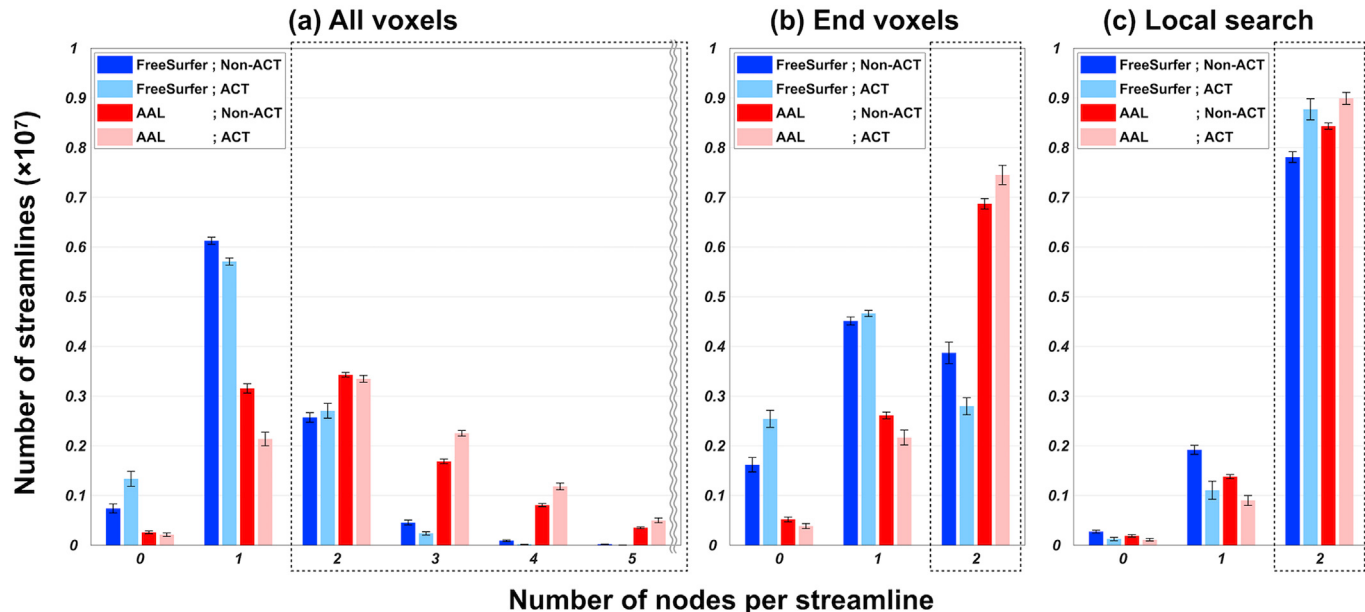


Fig. 3. Histograms of node count per streamline derived from the HCP data following 12 connectome construction strategies, where streamlines were assigned to brain nodes based on the (a) “all voxels”; (b) “end voxels”; (c) “local search” assignment mechanisms (see Methods 2.2.D for detailed descriptions). The horizontal axis shows the node count, and the vertical axis shows the group-averaged streamline count (mean \pm standard deviation). The dotted box shown in each plot indicates that the relevant streamlines have actual contributions to the outcome connectivity matrices.

edge intensities of using AAL atlas are greater than using FreeSurfer parcellations (i.e. compared on the same column), as the AAL nodes have greater spatial coverage or volume in general. For the same parcellation scheme (i.e. compared on the same row), all connectomes display similar global patterns but have visible alterations in edge intensities. Overall, the use of ACT results in greater edge intensities than non-ACT both intra- and inter-hemispherically. Also, there are observable discrepancies between node assignment methods, either with or without the application of ACT. Relatively speaking, the “end voxel” assignment has the lowest edge intensities than the “all voxels” and the “local search” method.

3.3. DMN connectivity & graph theory metrics

Tables 1 and 2 show the outcomes of DMN connectivity and global network metrics computed from the in-house data respectively. The results are summarised as follows:

- **Tracking termination criteria** – For each given node assignment mechanism, nearly all network metrics were significantly different between the use or non-use of ACT, regardless of the parcellation scheme used.

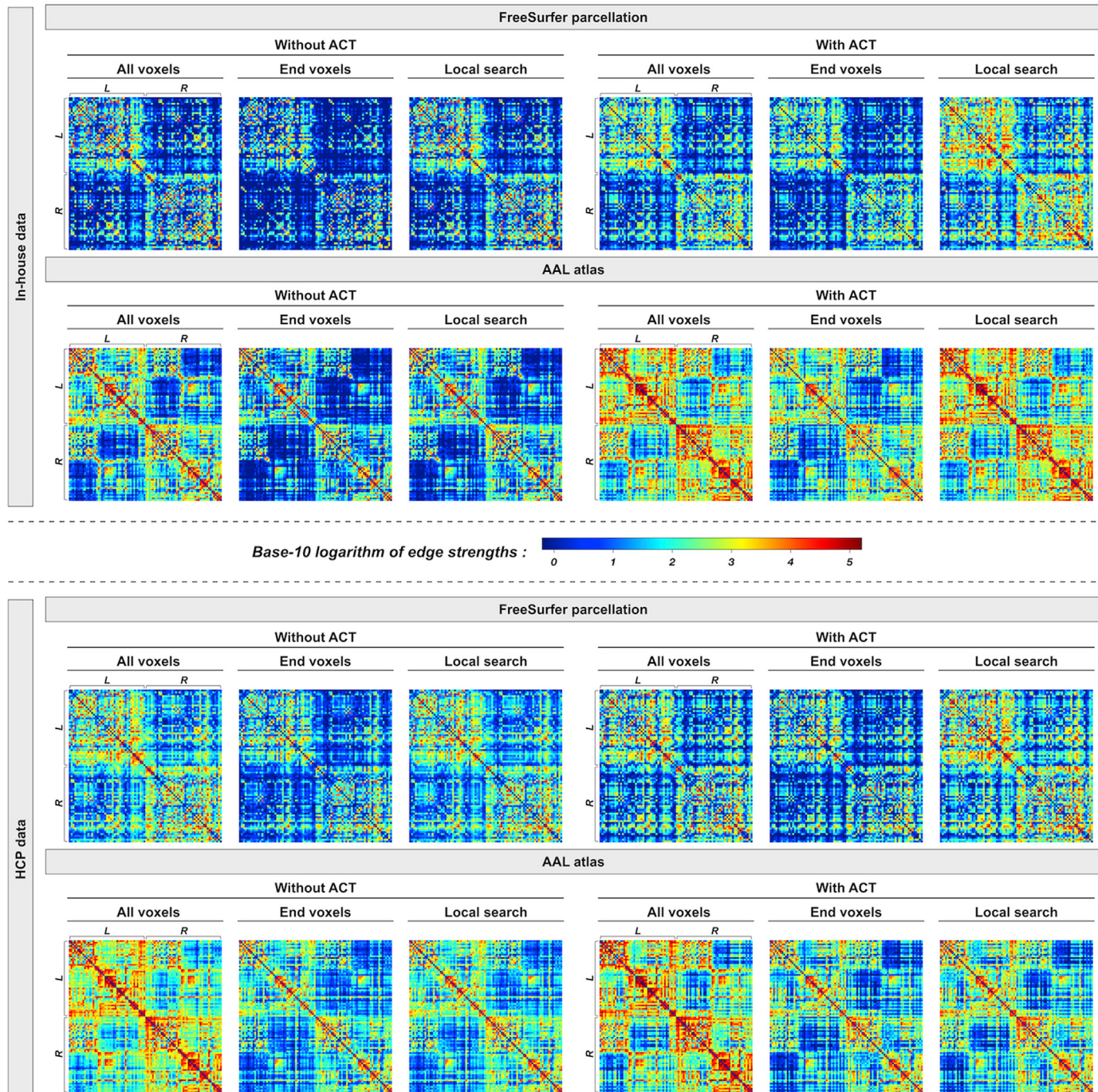


Fig. 4. Group-averaged connectivity matrices displayed in base-10 logarithm scale. The upper two rows are the connectomes obtained from the in-house MRI data, and bottom two rows are from the HCP MRI data. In each dataset, the first and the second row use the FreeSurfer parcellation and the AAL atlas respectively. In each row, the matrices are obtained using tractography either without ACT or with ACT, where three node assignment mechanisms (“all voxels”, “end voxels”, and “local search”) are used for each tractography method. The connectome edges show weighted streamline counts, as computed by the sum of streamline weights modulated using SIFT2. The letter ‘L’ and ‘R’ denote left and right hemisphere respectively.

Table 1

Mean and standard deviation values of the connection strengths of the default mode networks (DMN) derived from 22 in-house datasets.

Parcellation		FreeSurfer parcellations					
Metrics		Without ACT			With ACT		
		All voxels	End voxels	Local search	All voxels	End voxels	Local search
$S_{DMN\text{-}intra}$		13.19 ± 2.80	4.58 ± 0.91 ^Ψ	12.11 ± 1.89 ^Ω	7.55 ± 1.51*	4.28 ± 0.99 ^Ψ	29.41 ± 2.87 ^{ΦΩ*}
$S_{DMN\text{-}inter}$		69.42 ± 11.19	25.61 ± 3.69 ^Ψ	72.54 ± 7.13 ^Ω	40.81 ± 8.49*	24.83 ± 5.50 ^Ψ	164.10 ± 10.34 ^{ΦΩ*}

Parcellation		AAL atlas					
Metrics		Without ACT			With ACT		
		All voxels	End voxels	Local search	All voxels	End voxels	Local search
$S_{DMN\text{-}intra}$		39.17 ± 7.39	10.79 ± 1.54 ^Ψ	12.58 ± 1.66 ^{ΦΩ}	95.12 ± 23.47*	10.10 ± 1.51 ^Ψ	12.11 ± 1.74 ^{ΦΩ}
$S_{DMN\text{-}inter}$		155.99 ± 29.08	37.42 ± 4.13 ^Ψ	46.69 ± 4.34 ^{ΦΩ}	490.45 ± 93.39*	74.03 ± 7.65 ^{Ψ*}	90.48 ± 7.36 ^{ΦΩ*}

The values indicate the total connection strength ($\times 10^4$). Significant differences (Bonferroni-corrected $p < 0.05/9$) are denoted by: (i) $Ψ$ for “all voxels” versus “end voxels”, labelled at the side of “end voxels”; (iii) $Φ$ for “all voxels” versus “local search”, labelled at the side of “local search”; (ii) $Ω$ for “end voxels” versus “local search”, labelled at the side of “local search”; (iv) * for non-ACT versus ACT using the same assignment mechanism, labelled at the side of each assignment method with ACT. See [Supplementary Fig. S2](#) for the results of node-wise connectivity strengths.

Table 2

Mean and standard deviation values for network metrics derived from 22 in-house datasets.

Parcellation		FreeSurfer parcellations					
Metrics		Without ACT			With ACT		
		All voxels	End voxels	Local search	All voxels	End voxels	Local search
ρ	(%)	73.80 ± 9.30	60.00 ± 8.34 ^Ψ	75.58 ± 7.22 ^Ω	83.68 ± 2.98*	78.58 ± 3.20 ^{Ψ*}	92.66 ± 2.25 ^{ΦΩ*}
K^W	($\times 10^4$)	5.18 ± 0.96	1.93 ± 0.32 ^Ψ	5.39 ± 0.67 ^Ω	3.21 ± 0.55*	1.90 ± 0.37 ^Ψ	10.61 ± 0.48 ^{ΦΩ*}
B^W	($\times 10^{-2}$)	5.06 ± 0.23	5.20 ± 0.35	5.20 ± 0.29	3.79 ± 0.26*	3.84 ± 0.30 *	3.31 ± 0.29 ^{ΦΩ*}
C^W	($\times 10^{-2}$)	8.91 ± 1.25	7.83 ± 1.45	9.06 ± 1.26 ^Ω	8.11 ± 1.17	8.09 ± 1.41	11.47 ± 2.03 ^{ΦΩ*}
L^W	($\times 10^{-4}$)	5.28 ± 0.97	14.13 ± 2.11 ^Ψ	5.01 ± 0.53 ^Ω	13.43 ± 3.02*	23.64 ± 5.46 ^{Ψ*}	3.38 ± 0.31 ^{ΦΩ}
E_G^W	($\times 10^{-2}$)	6.72 ± 1.12	5.31 ± 1.08 ^Ψ	6.59 ± 1.05 ^Ω	4.95 ± 0.84*	4.78 ± 0.89	8.21 ± 1.33 ^{ΦΩ*}
E_L^W	($\times 10^{-3}$)	7.51 ± 1.46	7.11 ± 1.90	7.27 ± 1.31	8.94 ± 1.49*	8.88 ± 1.75 *	13.46 ± 2.21 ^{ΦΩ*}

Parcellation		AAL atlas					
Metrics		Without ACT			With ACT		
		All voxels	End voxels	Local search	All voxels	End voxels	Local search
ρ	(%)	91.35 ± 5.54	79.27 ± 7.08 ^Ψ	84.77 ± 5.77 ^Φ	98.80 ± 0.79*	94.21 ± 1.78 ^{Ψ*}	96.56 ± 1.24 ^{ΦΩ*}
K^W	($\times 10^4$)	16.46 ± 2.42	5.39 ± 0.46 ^Ψ	6.96 ± 0.49 ^{ΦΩ}	44.13 ± 5.68*	8.81 ± 0.53 ^{Ψ*}	11.13 ± 0.54 ^{ΦΩ*}
B^W	($\times 10^{-2}$)	4.76 ± 0.21	5.46 ± 0.31 ^Ψ	5.33 ± 0.27 ^Φ	3.72 ± 0.25*	3.44 ± 0.26 ^{Ψ*}	3.34 ± 0.25 ^{Φ*}
C^W	($\times 10^{-2}$)	10.16 ± 0.59	7.20 ± 1.14 ^Ψ	7.31 ± 0.93 ^Φ	12.35 ± 1.18*	8.57 ± 1.45 ^{Ψ*}	9.09 ± 1.42 ^{Φ*}
L^W	($\times 10^{-4}$)	1.97 ± 0.25	5.55 ± 0.51 ^Ψ	4.27 ± 0.34 ^{ΦΩ}	0.96 ± 0.12*	4.71 ± 0.37 ^{Ψ*}	3.62 ± 0.28 ^{ΦΩ*}
E_G^W	($\times 10^{-2}$)	8.18 ± 0.62	5.61 ± 0.93 ^Ψ	5.90 ± 0.80 ^Φ	8.88 ± 1.01	6.31 ± 1.00 ^Ψ	7.04 ± 1.00 ^{Φ*}
E_L^W	($\times 10^{-3}$)	9.99 ± 1.18	5.94 ± 1.07 ^Ψ	6.54 ± 0.94 ^Φ	16.25 ± 2.67*	11.53 ± 2.07 ^{Ψ*}	13.72 ± 2.24 ^{ΦΩ*}

Significant differences (Bonferroni-corrected $p < 0.05/9$) are denoted by: (i) $Ψ$ for “all voxels” versus “end voxels”, labelled at the side of “end voxels”; (iii) $Φ$ for “all voxels” versus “local search”, labelled at the side of “local search”; (ii) $Ω$ for “end voxels” versus “local search”, labelled at the side of “local search”; (iv) * for non-ACT versus ACT using the same assignment mechanism, labelled at the side of each assignment method with ACT.

- **Node assignment mechanisms** – For both parcellation schemes, most of the network metrics were altered significantly by changing the mechanism used to assign streamlines to nodes, both with and without the use of ACT.

Tables 3 and 4 show the outcomes obtained from the HCP data. Similar to the tendency observed in the results from the in-house data: a) no matter which node assignment approach was used, significant differences were observed in most network metrics between non-ACT and ACT for both FreeSurfer and AAL parcellation schemes; b) the network metrics differed significantly between the node assignment mechanisms.

4. Discussion

This study demonstrates that tractogram-based connectome construction can be strongly influenced by several confounding factors in the process of assigning streamlines to nodes. The relevant strategies concerning how to assign streamlines to the associated network nodes are seldom reported in studies using this technique; however, our data reveal that these most fundamental strategies have non-trivial substantive consequences for connectome quantification.

For connectome construction, the spatial extent of a node defined by an image-based brain parcellation scheme can have convoluted interactions with the criteria used to terminate a streamline, as well as the mechanism used to assign a streamline to the relevant nodes. We have shown that a simple change in the selection of brain parcellation scheme, the criteria of tractography termination, or the strategy of assigning streamlines to nodes can induce significant variation in the construction of structural connectivity. The resultant pairwise connectivity, as well as some of the most basic and commonly-used network metrics, are significantly affected by the methods used to generate streamlines tractograms and structural connectomes, suggesting that the whole process employed for connectome construction needs to be cautiously considered.

Furthermore, our results also reveal that even in the case of state-of-the-art HCP data (Glasser et al., 2013; Van Essen et al., 2013) and with the use of an advanced MSMT-CSD (Jeurissen et al., 2014) modelling approach for improved estimates of FODs, the resultant streamlines connectivity and connectomic metrics are still significantly dependent on the mechanisms used to generate the connectome. This highlights the necessity to understand the details of this process and its efficacy when applied to particular reconstructions; improved data quality (e.g. the

Table 3

Mean and standard deviation values of the connection strengths of the default mode networks (DMN) derived from 10 HCP datasets.

Parcellation		FreeSurfer parcellations					
Metrics		Without ACT			With ACT		
		All voxels	End voxels	Local search	All voxels	End voxels	Local search
$S_{DMN\text{-}intra}$		21.97 ± 3.79	10.12 ± 1.79 ^w	19.04 ± 2.21 ^Ω	17.46 ± 1.86*	8.25 ± 0.87 ^w	32.02 ± 2.83 ^{ΦΩ*}
$S_{DMN\text{-}inter}$		132.08 ± 9.85	57.76 ± 5.39 ^w	111.25 ± 5.32 ^{ΦΩ}	112.85 ± 7.94*	54.27 ± 5.25 ^w	185.62 ± 10.14 ^{ΦΩ*}

Parcellation		AAL atlas					
Metrics		Without ACT			With ACT		
		All voxels	End voxels	Local search	All voxels	End voxels	Local search
$S_{DMN\text{-}intra}$		84.87 ± 9.83	9.60 ± 0.99 ^w	11.50 ± 1.15 ^{ΦΩ}	119.11 ± 17.15*	12.64 ± 1.12 ^{w*}	14.54 ± 1.34 ^{ΦΩ*}
$S_{DMN\text{-}inter}$		412.86 ± 38.20	53.45 ± 2.62 ^w	65.23 ± 2.63 ^{ΦΩ}	604.47 ± 69.33*	85.64 ± 4.31 ^{w*}	101.15 ± 4.52 ^{ΦΩ*}

The values indicate the total connection strength ($\times 10^4$). Significant differences (Bonferroni-corrected $p < 0.05/9$) are denoted by: (i) ^w for “all voxels” versus “end voxels”, labelled at the side of “end voxels”; (iii) ^Φ for “all voxels” versus “local search”, labelled at the side of “local search”; (ii) ^Ω for “end voxels” versus “local search”, labelled at the side of “local search”; (iv) * for non-ACT versus ACT using the same assignment mechanism, labelled at the side of each assignment method with ACT. See [Supplementary Fig. S3](#) for the results of node-wise connectivity strengths.

Table 4

Mean and standard deviation values for network metrics derived from 10 HCP datasets.

Parcellation		FreeSurfer parcellations					
Metrics		Without ACT			With ACT		
		All voxels	End voxels	Local search	All voxels	End voxels	Local search
ρ	(%)	96.54 ± 1.05	88.47 ± 1.70 ^w	96.08 ± 0.93 ^Ω	87.15 ± 1.61*	80.19 ± 1.95 ^{w*}	92.92 ± 1.33 ^{ΦΩ*}
K^W	($\times 10^4$)	9.60 ± 0.85	3.50 ± 0.31 ^w	7.36 ± 0.30 ^{ΦΩ}	7.77 ± 0.51*	3.53 ± 0.25 ^w	12.04 ± 0.42 ^{ΦΩ*}
B^W	($\times 10^{-2}$)	4.45 ± 0.25	5.07 ± 0.51 ^w	4.96 ± 0.47	4.57 ± 0.37	4.45 ± 0.36	4.37 ± 0.34*
C^W	($\times 10^{-2}$)	9.21 ± 0.74	7.75 ± 0.77 ^w	8.39 ± 0.63	7.55 ± 1.12*	6.63 ± 1.07	8.83 ± 0.73 ^Ω
L^W	($\times 10^{-4}$)	2.93 ± 0.24	9.48 ± 0.82 ^w	3.96 ± 0.16 ^{ΦΩ}	4.87 ± 0.78*	14.40 ± 3.27 ^{w*}	2.60 ± 0.09 ^{ΦΩ*}
E_G^W	($\times 10^{-2}$)	7.42 ± 0.55	4.58 ± 0.41 ^w	5.90 ± 0.42 ^{ΦΩ}	4.68 ± 0.76*	3.39 ± 0.71 ^{w*}	6.13 ± 0.50 ^{ΦΩ}
E_L^W	($\times 10^{-3}$)	10.29 ± 0.90	5.66 ± 0.51 ^w	7.56 ± 0.50 ^{ΦΩ}	6.69 ± 1.10*	5.15 ± 1.10	9.16 ± 0.67 ^{ΦΩ*}

Parcellation		AAL atlas					
Metrics		Without ACT			With ACT		
		All voxels	End voxels	Local search	All voxels	End voxels	Local search
ρ	(%)	99.74 ± 0.14	95.55 ± 1.00 ^w	97.82 ± 0.74 ^Φ	98.32 ± 1.03*	93.61 ± 1.36 ^{w*}	95.32 ± 1.07 ^{Φ*}
K^W	($\times 10^4$)	40.15 ± 2.45	6.91 ± 0.28 ^w	8.64 ± 0.34 ^{ΦΩ}	55.82 ± 4.00*	10.19 ± 0.40 ^{w*}	12.57 ± 0.37 ^{ΦΩ*}
B^W	($\times 10^{-2}$)	4.06 ± 0.21	5.23 ± 0.21 ^w	4.85 ± 0.17 ^{ΦΩ}	4.13 ± 0.19	4.65 ± 0.26 ^{w*}	4.22 ± 0.18 ^{Ω*}
C^W	($\times 10^{-2}$)	11.77 ± 0.78	7.17 ± 0.62 ^w	7.15 ± 0.56 ^Φ	12.45 ± 1.02	7.53 ± 0.59 ^w	7.88 ± 0.58 ^Φ
L^W	($\times 10^{-4}$)	0.92 ± 0.05	4.79 ± 0.17 ^w	3.91 ± 0.15 ^{ΦΩ}	0.72 ± 0.05*	3.76 ± 0.19 ^{w*}	3.01 ± 0.07 ^{ΦΩ*}
E_G^W	($\times 10^{-2}$)	9.36 ± 0.55	5.46 ± 0.46 ^w	5.72 ± 0.46 ^Φ	8.84 ± 0.69	5.26 ± 0.44 ^w	5.84 ± 0.46 ^Φ
E_L^W	($\times 10^{-3}$)	16.23 ± 1.39	7.44 ± 0.75 ^w	8.61 ± 0.89 ^{ΦΩ}	14.79 ± 1.51	8.35 ± 0.83 ^w	10.13 ± 1.00 ^{ΦΩ*}

Significant differences (Bonferroni-corrected $p < 0.05/9$) are denoted by: (i) ^w for “all voxels” versus “end voxels”, labelled at the side of “end voxels”; (iii) ^Φ for “all voxels” versus “local search”, labelled at the side of “local search”; (ii) ^Ω for “end voxels” versus “local search”, labelled at the side of “local search”; (iv) * for non-ACT versus ACT using the same assignment mechanism, labelled at the side of each assignment method with ACT.

extensively-used HCP datasets) is not in itself sufficient to alleviate this issue.

Although there is currently no ground-truth biological data (which is a widely recognised issue) to directly indicate which mechanism investigated in this study provides the results that best reflect biological reality, it is nevertheless possible to argue that in principle the outcomes derived from methods that address recognised fibre-tracking termination problems at the tractography stage should be more advantageous for subsequent connectome construction and analysis. In the following sections, we discuss the effects of the three investigated confounding factors on the construction of 2-node streamline connections and on the subsequent network analyses.

4.1. Construction of pairwise connections

4.1.1. Effect of brain parcellation scheme

The histograms shown in [Figs. 2 and 3](#) demonstrate that using the AAL atlas results in more 2-node connections than using FreeSurfer's parcellation, when the same approaches for streamline termination and node assignment are used. This is due to the presence of labelled WM voxels in the AAL ROIs, resulting in a higher likelihood of a streamline

reaching a labelled voxel, as opposed to when using FreeSurfer's parcellation scheme, where node labelling is entirely constrained to GM voxels. For the case without using ACT, such an increase in pairwise connections using AAL largely results from those tracks terminating prematurely within actual WM tissue regions but which nevertheless reach AAL parcels along their trajectories or at both endpoint voxels. Since such terminations are considered erroneous, the use of the AAL atlas should not be reasoned as an appropriate substitution for ACT, nor does it indicate that the AAL atlas is a more effective parcellation scheme than FreeSurfer's parcellations for connectome construction: as illustrated in [Fig. 5](#), some track endpoints that are unassignable in FreeSurfer's parcellation scheme ([Fig. 5\(a\)](#)) become assignable in AAL atlas ([Fig. 5\(b\)](#)), but the majority of those endpoints actually locate within brain WM ([Fig. 5\(c\)](#)).

For the case of ACT, there was also a notable increase in pairwise connections when using the AAL atlas rather than the FreeSurfer parcellation (e.g. [Fig. 2\(b\)](#): from ~23% to ~72% & [3\(b\)](#): from ~29% to ~75%). This improvement in frequency of 2-node connections mainly resulted from the increased overlap between the AAL atlas and the GMWMI where ACT enforces the streamline endpoints to reside, which alleviates the issue of image mismatch when using FreeSurfer's

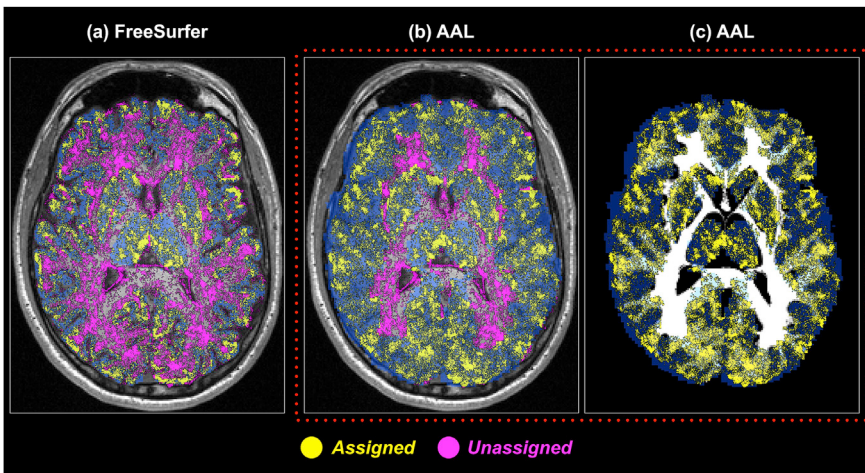


Fig. 5. The spatial distributions of success in assigning the streamline endpoints of non-ACT to brain network nodes using the “*end voxels*” assignment mechanism, demonstrated on in-house data. Streamline endpoints successfully assigned to a node are coloured in yellow and those unassigned are coloured in purple. (a–b) The assigned and unassigned endpoints are overlaid on a structural T1-weighted image when brain nodes (coloured in blue) are defined using (a) FreeSurfer parcellations; (b) the AAL atlas. (c) The background image in (b) is replaced by the WM partial volume map and only the assignable endpoints are shown, illustrating that many of those assigned streamline endpoints in fact terminated within brain WM. This suggests that a higher proportion of 2-node connections provided by a change from the FreeSurfer parcellation scheme to the AAL atlas cannot reflect biologically meaningful connectivity.

parcellations (see subsection D). However, the AAL atlas should not be considered as a requirement of ACT for constructing 2-node connections. The outcome of fewer 0- or 1-node connections in ACT than in non-ACT suggests that generating biologically-plausible track terminations is still a prerequisite for the application of a parcellation scheme with parcels not constrained to GM areas (e.g. the AAL atlas), as such a parcellation scheme does not in itself provide a meaningful compensation for the defect in both tracking terminations and assignment mechanism.

When using the AAL atlas, some studies incorporated a culling procedure that trimmed the excessive non-GM coverage of the AAL atlas during the process of connectome construction in order to discard the biologically inaccurate connections (i.e. streamlines not reaching GM areas) (Zalesky et al., 2010). Although this could avoid falsely assigning those invalid streamlines to AAL ROIs, such a processing step resulted in considerable low proportion of pairwise connectivity (~18%–33%) (Zalesky et al., 2010); their results were actually akin to the outcomes of using FreeSurfer's ROIs investigated in this study, i.e. when the nodes mostly represented brain GM (~32% for non-ACT, see Fig. 2(b)).

4.1.2. Effect of track termination criteria

The application of ACT has been demonstrated to have significant influence on a range of network metrics (Yeh et al., 2016). In this study, we not only investigated the downstream network metrics but also directly evaluated the frequency of pairwise connectivity given various types of parcellation schemes and node assignment mechanisms, based on both standard quality MRI data that is achievable on modern MRI scanners and high quality data from the HCP. Compared to non-ACT where streamlines can terminate erroneously within the brain (e.g. in CSF), ACT is designed to constrain track terminations to the GMWMI by using anatomical information as defined based on tissue PVMs (Smith et al., 2012). Such improvement in track termination is in principle more biologically reasonable and beneficial for identification of connectivity between GM ROIs; this is reflected by the overall increase in pairwise connections in most of the strategies for connectome construction (Figs. 2(c) and 3(c)).

Although ACT provides an overall improvement of streamline terminations by respecting the actual tissue anatomy, our results do however suggest that an appropriate node assignment mechanism is still needed in order to identify putative pairwise connections from both biologically-plausible endpoints. These endpoints cannot always be assigned to nodes based purely on the voxels in which the endpoints reside (Figs. 2(b) and 3(b)), as this would rely on the consistency between how brain tissue segmentation is used to terminate streamlines, and how a GM parcellation is defined (see subsection D below). In ACT, streamlines are terminated at the GMWMI as determined using trilinear interpolation of the tissue segmentation maps at the tractography stage; as such, the voxel of GMWMI in which the termination resides may not

always be labelled as GM within the parcellation (depending on the derivation of that parcellation), where a binary classification of each voxel is necessary (see Fig. 6 for visual demonstration). At the connectome construction stage, performing a heuristic “*local search*” (e.g. 2-mm used in this study) from meaningful track endpoints of ACT is intended to mitigate the effects of such small inconsistencies. Notably, the combination of ACT and “*local search*” provides the highest frequency (~90%) of pairwise connections for both datasets (Figs. 2(c) and 3(c)), and conveniently, this strategy enables the construction of 2-node connections to be robust with respect to different types of brain parcellation schemes. Supplementary Fig. S1 shows the outcome distributions of streamline endpoints that are the assignable or unassignable to brain nodes based on the utilisation of ACT and “*local search*”.

4.1.3. Effect of node assignment mechanism

The illustrative example shown in Fig. 1 demonstrates how the node assignment mechanism could easily affect the outcome of connectome quantification; this is consistent with the histogram results of node-count-per-streamline using both the in-house MRI data (Fig. 2) and the high-quality HCP data (Fig. 3). In practice, the mechanism by which individual streamlines contribute to the connectome can be ill-defined in many instances. For instance, when an individual streamline connects ≥ 3 nodes (which can in fact occur either with or without ACT, depending on the coverage of parcellation images; see Figs. 2(a) and 3(a)), the “*all voxels*” approach results in this streamline contributing to 3 or even more edges in the connectome. Not only does this lack biological plausibility, the limitations of current tractography techniques simply do not have the capability to provide such information in a robust manner regardless.

The detrimental consequence of the above is that if an inappropriate node assignment mechanism is used, properties of the resulting connectomes are likely to be dominated by the ill performance of that mechanism and its interaction with track termination criteria rather than realistic biology. Importantly, such a strong dependency on the streamline-to-node assignment approach cannot be overcome simply by the use of state-of-the-art modelling techniques and high-quality (e.g. HCP) MRI data (Fig. 3). The complexity of the node assignment problem reflects that assigning each streamline to *exactly* 2 brain nodes is in principle optimal; in addition, it is more advantageous to apply anatomical criteria for avoiding erroneous streamline terminations in the first place, rather than attempting to design a dedicated node assignment mechanism, as the latter alone is unlikely to take the variety of possible scenarios into consideration.

4.1.4. Effects of source data mismatch

Due to the partial volume effect inherent to image data, currently there is no universal principle to determine the *exact* location of the boundary between GM and WM. An image-based boundary derived from

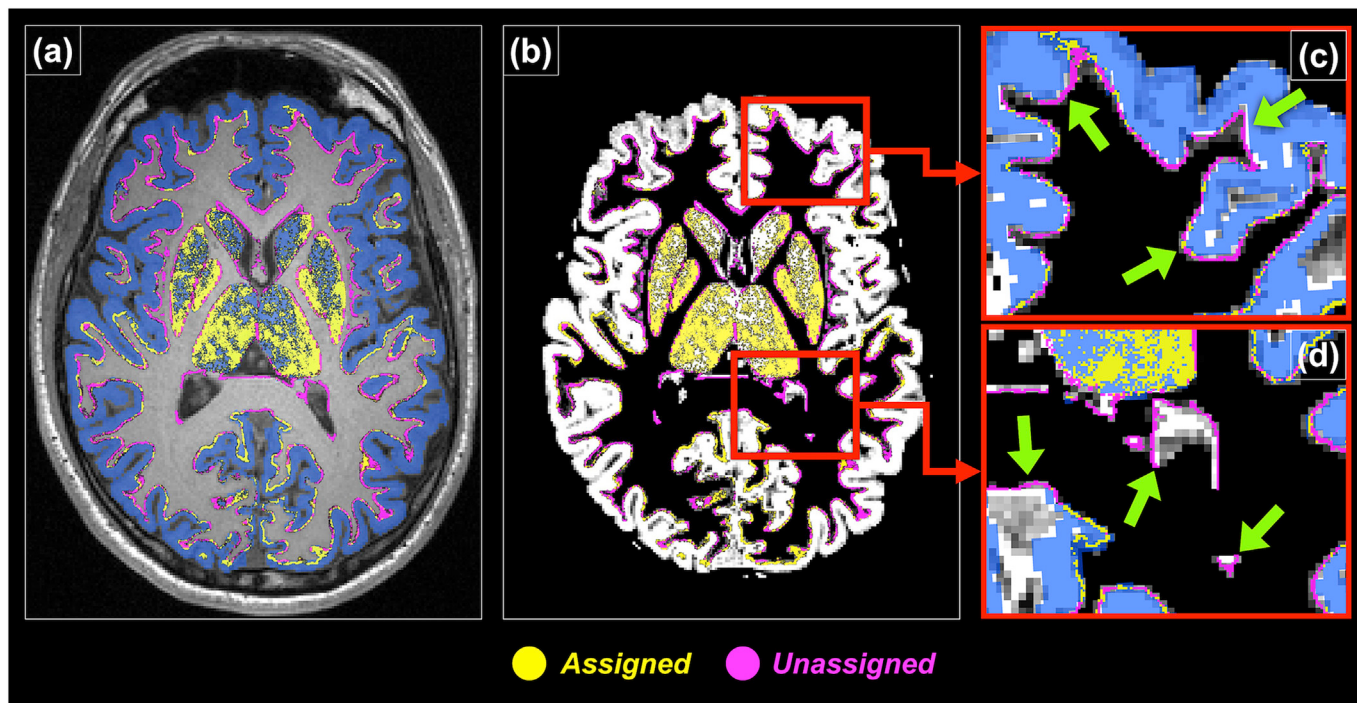


Fig. 6. Demonstration of misalignment between FreeSurfer parcellations and intensity-based tissue partial volume estimates. Streamline endpoints of ACT are assigned to brain network nodes using the “end voxels” assignment mechanism; endpoints are coloured yellow and purple upon successful and unsuccessful assignment to a brain node respectively. (a) With ACT, streamline endpoints occur either at the GM-WM interface, within the subcortical GM, or at the inferior edge of the spinal column (not visible here). Many of these endpoints (purple points) are not located inside a voxel designated by the FreeSurfer parcellation image (blue voxels) and thus are not assigned to a node. (b) The background T1-weighted image shown in (a) is replaced by the GM partial volume map derived from an intensity-based tissue segmentation. (c) & (d) Zoomed regions of (b) to further illustrate the discrepancy (pointed by arrows) between brain tissue segmentation and grey matter parcellation (See [Supplementary Fig. 1](#) for the case of using the “local search” assignment method).

brain tissue segmentation (i.e. voxels of tissue partial volume fractions) does not necessarily match with that from brain parcellation (i.e. voxels of labelled integer indices). In this study, when using ACT, streamlines are truncated at the GMWMI as defined based on trilinear interpolation of tissue partial volume estimates derived from FSL (i.e. as described in the original development of ACT ([Smith et al., 2012](#))). When using FreeSurfer’s cortical parcellations ([Desikan et al., 2006](#)), the images contain only discretely labelled parcels on the voxel grid and do not consider tissue partial volume fractions within voxels; moreover, parcel labelling is limited to voxels with substantial grey matter partial volume only. As illustrated by [Fig. 6\(c and d\)](#), ACT terminates streamlines due to reaching the estimated GMWMI; however, many voxels in which those terminations occur are not labelled by the FreeSurfer parcellation. This is reflected in our data where the “end voxels” approach was used to assign the track endpoints while using ACT (see [Figs. 2\(b\) and 3\(b\)](#)), where <35% of streamlines were assigned to 2 nodes.

It should be noted that fundamental algorithmic differences between tissue segmentation and brain parcellation also means that some cortical or deep brain structures that are classified as GM structures may not be labelled by FreeSurfer or the AAL atlas, as illustrated by [Fig. 6\(d\)](#). For example, the claustrum, a thin irregular layer of GM (or neurons) between the putamen and the insula, is typically omitted in brain parcellations since its size is too small to be accurately extracted even from high-resolution structural T1 image. These explain why there are ~10% of streamlines not assigned to 2 nodes when using ACT in conjunction with “local search” (see [Figs. 2\(c\) and 3\(c\)](#)), which is likely to result primarily from regions considered as GM PVM but not labelled by the FreeSurfer parcellation.

In principle, using the *same* source information at fibre-tracking and connectome construction could avoid the problem of source data mismatch. However, if performed naively, brain parcellation images would not constitute accurate anatomical constraints, as the binary

nature of structural labels (i.e. ‘voxelised’ or ‘staircase’ rather than partial volume fractions) would downgrade the accuracy of streamlines tractography. Furthermore, since there are some known GM structures not represented in labelled images, either a) fibre tracking would continue at those GM regions where streamlines would ideally be terminated, or b) streamlines that attempt to terminate within actual GM areas would be unfavourably discarded by the anatomical criteria. Both scenarios would lead to invalid connectivity inferences.

4.2. Implications for network analysis

Our results demonstrate that the fundamental characteristics of the connectome can be heavily influenced by both the mechanism of streamlines termination, and the mechanism used to assign streamlines to nodes associated with the brain parcellation. These processes are frequently overlooked, but are in practice non-trivial and can alter connectomic measures significantly, even when using state-of-the-art HCP datasets and advanced data processing techniques. Any connectome constructed based on heuristic mechanisms where the majority of reconstructed streamlines do not contribute to the connectome is unlikely to provide an appropriate representation of the underlying fibre connectivity. From the examples and data presented in this study, it is beneficial to use mechanisms that are specifically tailored to correct for recognised inaccuracies of tractogram and connectome reconstruction, e.g. ACT to forbid erroneous streamline terminations and “local search” to account for inconsistencies between terminations and parcellations; this is supported by the increased frequency of successfully assigning each streamline to exactly two nodes when these methods are used in conjunction, independently of the parcellation scheme used ([Figs. 2\(c\) and 3\(c\)](#): ~90%; see also [Supplementary Fig. S1](#)). Network connectivity and graph theory metrics derived using these advanced mechanisms should therefore be in principle the most trustworthy results among all

strategies evaluated (Tables 1–4, last column), and therefore any significant deviations from these values imply potential biases introduced by the use of inappropriate connectome construction techniques.

In addition, our results suggest that without an appropriate strategy for assigning streamlines to parcellation nodes, network connectivity and graph theory metrics are altered significantly, despite all connectomes having been constructed from tractograms with quantitative properties provided via the SIFT2 method (Tables 1–4). This indicates that even though quantitative tractography methods are necessary for quantification of the structural connectome and network metrics derived thereof, these tractogram properties are likely to be lost during connectome construction if the streamline-to-node assignment process is not sufficiently robust. This observation is likely to remain if SIFT2 were to be replaced by other alternative quantitative processing methods (Christiaens et al., 2015; Daducci et al., 2015; Girard et al., 2017; Pestilli et al., 2014; Reisert et al., 2011; Sherbondy et al., 2008; Smith et al., 2013), as the algorithms of these methods are independent of the mechanism used for streamline-to-node-assignment.

A related question is whether it would be more appropriate to apply the quantitative tractogram filtering techniques only to the tractogram data that contribute to connectome quantification. For an ideal case, if a brain parcellation scheme comprehensively labels all the brain ROIs, then all streamlines should contribute to the connectome. However, as long as there are genuine brain GM areas not labelled by the parcellation (i.e. “latent” brain nodes), streamlines generated to represent the connectivity between these regions would be discarded. As a result, deficiencies in streamlines density relative to the image data along those ‘missing’ WM pathways would then be compensated by assigning stronger weights to other streamlines trajectories that traverse nearby the omitted pathway, consequently affecting connectome characteristics. Therefore, in order to avoid diminishing the benefits of quantitative tractogram reconstruction methods, we advocate applying these techniques to the whole-brain tractogram, even if not all streamlines go on to contribute to the connectome.

4.3. Limitations

Our results suggest that the incorporation of ACT and “*local search*” provide relatively robust construction of pairwise connectivity for different parcellation schemes. However, we do recognise that the “*local search*” assignment remains a simple heuristic to deal with the inconsistencies between tissue segmentations and brain parcellations. Since the discrepancy between GMWMI (derived from tissue segmentation maps) and brain parcellations does not appear to be evenly distributed across the brain (as illustrated in Fig. 6), it is difficult to determine a local searching distance that is effectively appropriate for all brain areas; decreasing the distance may omit putative WM connectivity, whereas lengthening the distance may be accompanied by an increase in false assignments (e.g. track endpoints at the claustrum could be assigned to neighbouring labelled structures). In addition, the reliability of “*local search*” depends on the accuracy of brain tissue segmentations that are typically used as anatomical constraints for fibre-tracking termination in advanced tractography algorithms (Girard et al., 2014; Smith et al., 2012), and thus inaccurate segmentations could potentially introduce bias in connectome quantification. When using an intensity-based segmentation technique (e.g. FSL’s FAST (Zhang et al., 2001)), a brain area that has a T1 value close to GM (e.g. T1 of an artery ~1500 ms at 3T) might be misclassified with a high GM volume fraction. Likewise, a voxel partially occupied by CSF and WM (such as the areas surrounding lateral ventricles) could also lead to a signal intensity that is equivalent to GM. Hence, when using such tissue segmentations to delineate the GMWMI, streamlines might terminate erroneously at those “pseudo” GM areas, and then be falsely assigned to neighbouring (genuine) node voxels via “*local search*” (depending on the maximal search radius used). The present study is limited to the use of FSL’s FAST for generating brain tissue PVMs, as applied in the ACT framework. Further studies on the

assessment of ACT incorporated with other tissue segmentation methods (Dora et al., 2017) are required to evaluate the robustness of tractogram reconstruction, which is beyond the scope of this study. Indeed, improving the quality of tissue segmentation and developing more sophisticated algorithms for streamline-to-node assignment would be beneficial for connectome construction; however, appropriate tracking termination is still a prerequisite step for building meaningful streamline connections nonetheless.

5. Conclusion

The strategies by which individual streamlines are terminated, and subsequently contribute to a particular edge in a connectome, have significant flow-through influences on derived structural network characteristics. The interactions between the brain parcellation schemes, the tractography termination criteria, and the assignment of individual streamlines cannot be addressed exclusively by the use of high quality MRI data. Hence, the underlying mechanisms need to be considered and explicitly stated in the tractogram-based structural connectomics. Recognition of the source of the problem enables selection of advanced processing approaches that potentially provide more trustworthy results for structural connectomics. It is essential to ensure that the algorithms used for track termination and brain parcellation are compatible, since inconsistencies in these can lead to substantially biased connectomes.

Acknowledgments

We are grateful to the National Health and Medical Research Council (NHMRC) of Australia, the Australian Research Council (ARC), and the Victorian Government’s Operational Infrastructure Support Program for their support. C.-H. Yeh is supported by a Postdoctoral Research Abroad Fellowship funded by Taiwan Ministry of Science and Technology (MOST 105-2917-I-564-040). Data were provided in part by the Human Connectome Project, WU-Minn Consortium (Principal Investigators: David Van Essen and Kamil Ugurbil; 1U54MH091657) funded by the 16 NIH Institutes and Centers that support the NIH Blueprint for Neuroscience Research; and by the McDonnell Center for Systems Neuroscience at Washington University.

Appendix A. Supplementary data

Supplementary data to this article can be found online at <https://doi.org/10.1016/j.neuroimage.2019.05.005>.

References

- Andersson, J.L.R., Skare, S., Ashburner, J., 2003. How to correct susceptibility distortions in spin-echo echo-planar images: application to diffusion tensor imaging. *Neuroimage* 20, 870–888.
- Andersson, J.L.R., Sotiroopoulos, S.N., 2016. An integrated approach to correction for off-resonance effects and subject movement in diffusion MR imaging. *Neuroimage* 125, 1063–1078.
- Buckner, R.L., Andrews-Hanna, J.R., Schacter, D.L., 2008. The brain’s default network: anatomy, function, and relevance to disease. *Ann. N. Y. Acad. Sci.* 1124, 1–38.
- Bullmore, E., Sporns, O., 2009. Complex brain networks: graph theoretical analysis of structural and functional systems. *Nat. Rev. Neurosci.* 10, 186–198.
- Christiaens, D., Reisert, M., Dhollander, T., Sunaert, S., Suetens, P., Maes, F., 2015. Global tractography of multi-shell diffusion-weighted imaging data using a multi-tissue model. *Neuroimage* 123, 89–101.
- Daducci, A., Dal Palù, A., Lemkadem, A., Thiran, J.-P., 2015. COMMIT: convex optimization modeling for microstructure informed tractography. *IEEE Trans. Med. Imaging* 34, 246–257.
- Dale, A.M., Fischl, B., Sereno, M.I., 1999. Cortical surface-based analysis. I. Segmentation and surface reconstruction. *Neuroimage* 9, 179–194.
- Desikan, R.S., Ségonne, F., Fischl, B., Quinn, B.T., Dickerson, B.C., Blacker, D., Buckner, R.L., Dale, A.M., Maguire, R.P., Hyman, B.T., Albert, M.S., Killiany, R.J., 2006. An automated labeling system for subdividing the human cerebral cortex on MRI scans into gyral based regions of interest. *Neuroimage* 31, 968–980.
- Dora, L., Agrawal, S., Panda, R., Abraham, A., 2017. State-of-the-Art methods for brain tissue segmentation: a Review. *IEEE Rev. Biomed. Eng.* 10, 235–249.
- Friston, K.J., Ashburner, J.T., Kiebel, S.J., Nichols, T.E., Penny, W.D., 2007. Statistical Parametric Mapping: the Analysis of Functional Brain Images. Academic Press.

- Girard, G., Daducci, A., Petit, L., Thiran, J.-P., Whittingstall, K., Deriche, R., Wassermann, D., Descoteaux, M., 2017. AxTract: toward microstructure informed tractography. *Hum. Brain Mapp.* 38, 5485–5500.
- Girard, G., Whittingstall, K., Deriche, R., Descoteaux, M., 2014. Towards quantitative connectivity analysis: reducing tractography biases. *Neuroimage* 98, 266–278.
- Glasser, M.F., Sotiroopoulos, S.N., Wilson, J.A., Coalson, T.S., Fischl, B., Andersson, J.L., Xu, J., Jbabdi, S., Webster, M., Polimeni, J.R., Van Essen, D.C., Jenkinson, M., WU-Minn HCP Consortium, 2013. The minimal preprocessing pipelines for the Human Connectome Project. *Neuroimage* 80, 105–124.
- Hagmann, P., Cammoun, L., Gigandet, X., Meuli, R., Honey, C.J., Wedeen, V.J., Sporns, O., 2008. Mapping the structural core of human cerebral cortex. *PLoS Biol.* 6, e159.
- Jeurissen, B., Tournier, J.-D., Dhollander, T., Connelly, A., Sijbers, J., 2014. Multi-tissue constrained spherical deconvolution for improved analysis of multi-shell diffusion MRI data. *Neuroimage* 103, 411–426.
- Lo, C.-Y., Wang, P.-N., Chou, K.-H., Wang, J., He, Y., Lin, C.-P., 2010. Diffusion tensor tractography reveals abnormal topological organization in structural cortical networks in Alzheimer's disease. *J. Neurosci.* 30, 16876–16885.
- Mugler, J.P., Brookeman, J.R., 1990. Three-dimensional magnetization-prepared rapid gradient-echo imaging (3D MP RAGE). *Magn. Reson. Med.* 15, 152–157.
- Patenaude, B., Smith, S.M., Kennedy, D.N., Jenkinson, M., 2011. A Bayesian model of shape and appearance for subcortical brain segmentation. *Neuroimage* 56, 907–922.
- Pestilli, F., Yeatman, J.D., Rokem, A., Kay, K.N., Wandell, B.A., 2014. Evaluation and statistical inference for human connectomes. *Nat. Methods* 11, 1058–1063.
- Raffelt, D., Tournier, J.D., Rose, S., Ridgway, G.R., Henderson, R., Crozier, S., Salvado, O., Connelly, A., 2012. Apparent Fibre Density: a novel measure for the analysis of diffusion-weighted magnetic resonance images. *Neuroimage* 59, 3976–3994.
- Reese, T.G., Heid, O., Weisskoff, R.M., Wedeen, V.J., 2003. Reduction of eddy-current-induced distortion in diffusion MRI using a twice-refocused spin echo. *Magn. Reson. Med.* 49, 177–182.
- Reisert, M., Mader, I., Anastasopoulos, C., Weigel, M., Schnell, S., Kiselev, V., 2011. Global fiber reconstruction becomes practical. *Neuroimage* 54, 955–962.
- Rubinov, M., Sporns, O., 2010. Complex network measures of brain connectivity: uses and interpretations. *Neuroimage* 52, 1059–1069.
- Sherbondy, A.J., Dougherty, R.F., Ben-Shachar, M., Napel, S., Wandell, B.A., 2008. ConTrack: finding the most likely pathways between brain regions using diffusion tractography. *J. Vis.* 8, 15.1–16.
- Smith, R.E., Tournier, J.-D., Calamante, F., Connelly, A., 2015a. The effects of SIFT on the reproducibility and biological accuracy of the structural connectome. *Neuroimage* 104, 253–265.
- Smith, R.E., Tournier, J.-D., Calamante, F., Connelly, A., 2015b. SIFT2: enabling dense quantitative assessment of brain white matter connectivity using streamlines tractography. *Neuroimage* 119, 338–351.
- Smith, R.E., Tournier, J.-D., Calamante, F., Connelly, A., 2013. SIFT: spherical deconvolution informed filtering of tractograms. *Neuroimage* 67, 298–312.
- Smith, R.E., Tournier, J.-D., Calamante, F., Connelly, A., 2012. Anatomically-constrained tractography: improved diffusion MRI streamlines tractography through effective use of anatomical information. *Neuroimage* 62, 1924–1938.
- Smith, S.M., Jenkinson, M., Woolrich, M.W., Beckmann, C.F., Behrens, T.E.J., Johansen-Berg, H., Bannister, P.R., De Luca, M., Drokbnjak, I., Flitney, D.E., Niazy, R.K., Saunders, J., Vickers, J., Zhang, Y., De Stefano, N., Brady, J.M., Matthews, P.M., 2004. Advances in functional and structural MR image analysis and implementation as FSL. *Neuroimage* 23 (Suppl. 1), S208–S219.
- Tournier, J.D., Calamante, F., Connelly, A., 2010. Improved probabilistic streamlines tractography by 2nd order integration over fibre orientation distributions. *Proc. Int. Soc. Magn. Reson. Med.* 1670.
- Tournier, J.D., Calamante, F., Connelly, A., 2007. Robust determination of the fibre orientation distribution in diffusion MRI: non-negativity constrained super-resolved spherical deconvolution. *Neuroimage* 35, 1459–1472.
- Tournier, J.D., Smith, R.E., Raffelt, D.A., Tabbara, R., Dhollander, T., Pietsch, M., Christiaens, D., Jeurissen, B., Yeh, C.-H., Connelly, A., 2019. MRtrix3: a fast, flexible and open software framework for medical image processing and visualisation. *bioRxiv* 551739.
- Tournier, J.D., Yeh, C.-H., Calamante, F., Cho, K.-H., Connelly, A., Lin, C.-P., 2008. Resolving crossing fibres using constrained spherical deconvolution: validation using diffusion-weighted imaging phantom data. *Neuroimage* 42, 617–625.
- Tustison, N.J., Avants, B.B., Cook, P.A., Zheng, Y., Egan, A., Yushkevich, P.A., Gee, J.C., 2010. N4ITK: improved N3 bias correction. *IEEE Trans. Med. Imaging* 29, 1310–1320.
- Tzourio-Mazoyer, N., Landeau, B., Papathanassiou, D., Crivello, F., Etard, O., Delcroix, N., Mazoyer, B., Joliot, M., 2002. Automated anatomical labeling of activations in SPM using a macroscopic anatomical parcellation of the MNI MRI single-subject brain. *Neuroimage* 15, 273–289.
- Van Essen, D.C., Smith, S.M., Barch, D.M., Behrens, T.E.J., Yacoub, E., Ügurbil, K., WU-Minn HCP Consortium, 2013. The Wu-minn human connectome Project: an overview. *Neuroimage* 80, 62–79.
- Yeh, C.-H., Smith, R.E., Liang, X., Calamante, F., Connelly, A., 2016. Correction for diffusion MRI fibre tracking biases: the consequences for structural connectomic metrics. *Neuroimage* 142, 150–162.
- Zalesky, A., Fornito, A., Harding, I.H., Cocchi, L., Yücel, M., Pantelis, C., Bullmore, E.T., 2010. Whole-brain anatomical networks: does the choice of nodes matter? *Neuroimage* 50, 970–983.
- Zhang, B., Horvath, S., 2005. A general framework for weighted gene co-expression network analysis. *Stat. Appl. Genet. Mol. Biol.* 4, Article17.
- Zhang, Y., Brady, M., Smith, S., 2001. Segmentation of brain MR images through a hidden Markov random field model and the expectation-maximization algorithm. *IEEE Trans. Med. Imaging* 20, 45–57.